

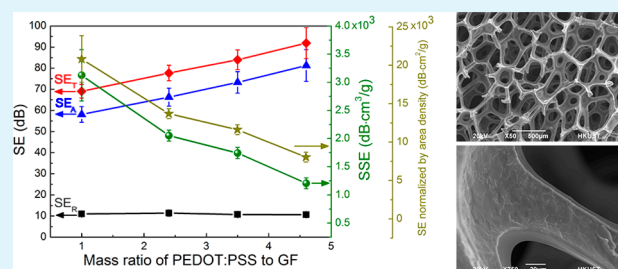
Ultralight Graphene Foam/Conductive Polymer Composites for Exceptional Electromagnetic Interference Shielding

Ying Wu,[†] Zhenyu Wang,[†] Xu Liu,[†] Xi Shen,[†] Qingbin Zheng,^{*,†,‡} Quan Xue,[§] and Jang-Kyo Kim^{*,†}[†]Department of Mechanical and Aerospace Engineering, The Hong Kong University of Science and Technology, Clear Water Bay, Kowloon, Hong Kong[‡]Institute for Advanced Study, The Hong Kong University of Science and Technology, Clear Water Bay, Kowloon, Hong Kong[§]Applied Electromagnetics Laboratory, Department of Electronic Engineering, City University of Hong Kong, Kowloon, Hong Kong

S Supporting Information

ABSTRACT: Ultralight, high-performance electromagnetic interference (EMI) shielding graphene foam (GF)/poly(3,4-ethylenedioxythiophene):poly(styrenesulfonate) (PEDOT:PSS) composites are developed by drop coating of PEDOT:PSS on cellular-structured, freestanding GFs. To enhance the wettability and the interfacial bonds with PEDOT:PSS, GFs are functionalized with 4-dodecylbenzenesulfonic acid. The GF/PEDOT:PSS composites possess an ultralow density of $18.2 \times 10^{-3} \text{ g/cm}^3$ and a high porosity of 98.8%, as well as an enhanced electrical conductivity by almost 4 folds from 11.8 to 43.2 S/cm after the incorporation of the conductive PEDOT:PSS. Benefiting from the excellent electrical conductivity, ultralight porous structure, and effective charge delocalization, the composites deliver remarkable EMI shielding performance with a shielding effectiveness (SE) of 91.9 dB and a specific SE (SSE) of $3124 \text{ dB}\cdot\text{cm}^3/\text{g}$, both of which are the highest among those reported in the literature for carbon-based polymer composites. The excellent electrical conductivities of composites arising from both the GFs with three-dimensionally interconnected conductive networks and the conductive polymer coating, as well as the left-handed composites with absolute permittivity and/or permeability larger than one give rise to significant microwave attenuation by absorption.

KEYWORDS: noncovalent functionalization, graphene foam composites, ultralightweight, EMI shielding, negative permittivity



1. INTRODUCTION

The widespread use of personal computers and portable electronics has resulted in severe electromagnetic interference (EMI) pollutions. EMI radiations in free spaces and radiation emanating from these pervasive sources are harmful to both human health and the normal operation of electronics. Therefore, various EMI-shielding materials have been developed to eliminate unwanted electromagnetic (EM) radiations as well as to protect neighboring components in electronic devices. For example, metallic mesh shields are often used in a smartphone to protect electronics from its cellular transmitter/receiver. In addition to high EMI shielding performance, easy processing and lightweights are among the key parameters required for the materials in many emerging areas like aerospace, aircraft, and automobiles.¹ Two typical materials, including (i) porous foam materials and (ii) conductive polymer composites (CPCs) containing conductive fillers, especially nanoscale carbon materials, have received much attention for lightweight and flexible EMI shielding applications. For example, the Cu–Ni alloy foams hybridized with carbon nanotubes (CNTs) had a low density of $\sim 0.25 \text{ g/cm}^3$ and showed a high EMI shielding effectiveness (SE) of $\sim 50 \text{ dB}$.² Although foamed metal-based composites present good SE values, they have a major drawback of relatively high

densities. CPCs reinforced with conductive carbon materials, such as carbon black,³ CNTs,⁴ carbon fibers,⁵ graphite,⁶ and graphene,⁷ delivered outstanding SE depending on their intrinsic properties, such as dielectric constants, electrical conductivities, and aspect ratios. Except for lightweights, carbon filler/polymer composites also possess unique advantages including ease of processing, low cost, tunable electric conductivities, and resistance to corrosion.⁸ Taking advantage of both the low-density, porous structure and the high electrical conductivity, CPC foams have attracted much attention in recent years for lightweight EMI shielding. Both high EMI SEs and high specific shielding effectiveness (SSE, SE per unit density) are reported for polymer-based aerogels reinforced with graphene^{9,10} and CNTs¹ because of the highly conductive fillers and the low density of porous structures. Despite the reduction of material density, porous structures are effective for the enhancement of EMI shielding performance.¹¹

Among different carbon/polymer composites, graphene reinforced CPCs appear to be the most effective for EMI shielding due to their excellent electrical conductivities, high

Received: January 20, 2017

Accepted: February 22, 2017

Published: February 22, 2017

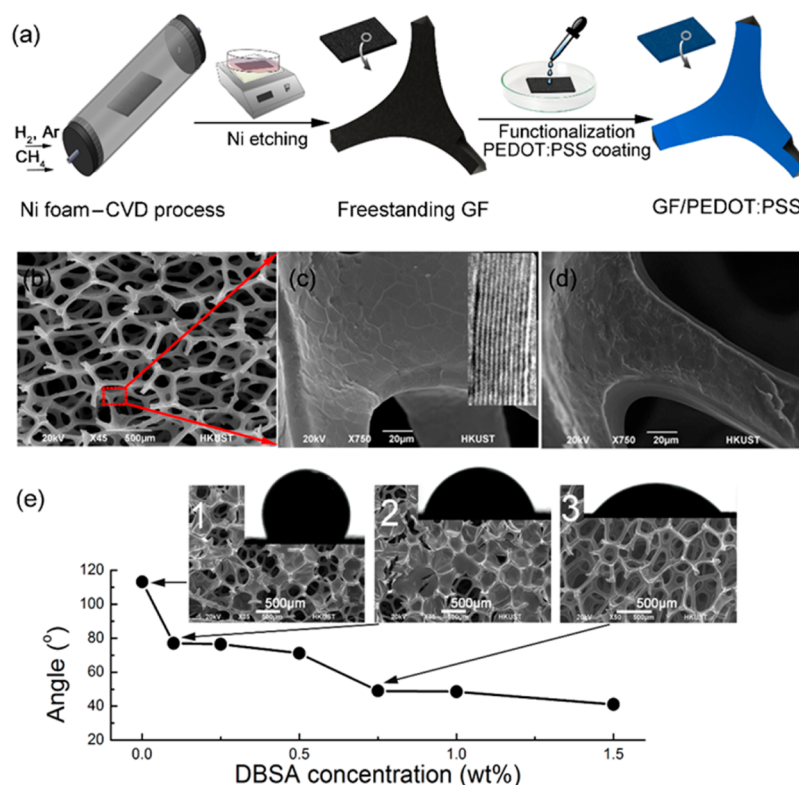


Figure 1. (a) Schematic procedure of the preparation of GF/PEDOT:PSS composites; SEM and TEM images of GFs (b, c) before and (d) after PEDOT:PSS coating and (e) contact angles of compressed GF plates as a function of DBSA concentration. The inset in (c) is the TEM image of pristine graphene. The insets in (e) show the SEM images of GF/PEDOT:PSS composites treated with different DBSA concentrations and the shapes of the corresponding PEDOT:PSS droplets (1, no treatment; 2, treated with 0.1 wt % DBSA; and 3, treated with 0.75 wt % DBSA).

electron mobility, and large specific surface areas. The aligned reduced graphene oxide (rGO)/epoxy composite with a filler content of 2 wt % exhibited a high EMI SE of 38 dB, although a relatively low SSE of 35.3 dB·cm³/g was obtained due to the large density of the solid composite structure.¹² When the densities of composites are reduced by incorporating porous fillers, the SSEs can be significantly improved. For example, an exceptional EMI SSE of ~500 dB·cm³/g was achieved by polydimethylsiloxane (PDMS) composites reinforced with graphene foam (GF) with an extremely low density of 0.06 g/cm³ which was grown by chemical vapor deposition (CVD).¹³ The formation of continuous conductive networks is another effective strategy for the improvement of EMI shielding SEs,¹⁵ which is mainly attributed to the high electrical conductivity and extensive dissipation of surface currents induced by EM waves. GFs with a continuous cellular structure were proven to be an excellent filler for polymer composites with excellent electrical and EMI shielding properties.^{13,15} The EMI shielding performance was further improved by introducing secondary conductive fillers, such as CNTs^{15,16} and metallic nanoparticles,¹⁷ or magnetic particles, such as Fe₃O₄,¹⁸ carbonyl iron,¹⁹ and Co₃O₄,²⁰ into the conducting composites. An extraordinary EMI SE of ~75 dB and a SSE of 833 dB·cm³/g were recently reported by adding CNTs into GF/PDMS composites.¹⁵ The addition of metallic and magnetic nanoparticles should be carefully designed for lightweight EMI shielding applications because of the sacrifice of density after the incorporation of these high-density particles.

It is worth noting that nonconductive polymers, such as epoxy, polystyrene (PS), PDMS, and poly(vinylidene fluoride) (PVDF), have been the main matrix materials employed to

fabricate graphene based CPCs for EMI applications. However, these polymers have inherently very low EMI SEs of smaller than 1 dB,^{15,21} making negligible contributions to the total EMI SEs of composites. Alternatively, intrinsically conducting polymers with high electrical conductivities and nontransparency to microwave radiation, such as polyaniline,²² polypyrrole,²³ and poly(3,4-ethylenedioxythiophene):poly(styrenesulfonate) (PEDOT:PSS),²⁴ are found to be an attractive choice as the matrix for effective EMI shielding composites. Conducting polymers have been widely used as coatings on nonconductive fabrics or textiles for EMI shielding. However, their EMI SEs were poor because of the low electrical conductivities and permittivities of the insulating fabrics.^{22,23} In view of the poor EMI shielding by conducting polymers alone, light weight carbon structures with high electrical conductivities and high porosities need to be incorporated to realize composites with desired light weights and EMI shielding characteristics.

This study is dedicated to development of GF/PEDOT:PSS composites with functionalities of easy processability, lightweight, high electrical conductivity, and superior EMI shielding properties. The composites were fabricated by drop coating of PEDOT:PSS aqueous solution on functionalized GFs. An ultralow density of 0.0182 g/cm³ and a high porosity of 98.8% were obtained for the composite with a GF weight fraction of 58%. The composite with an optimal composition gave rise to an excellent electrical conductivity of 43.2 S/cm and the corresponding total EMI SE of over 90 dB. These composites are particularly useful for mobile electronics and aerospace industries where lightweight materials/structures with highly

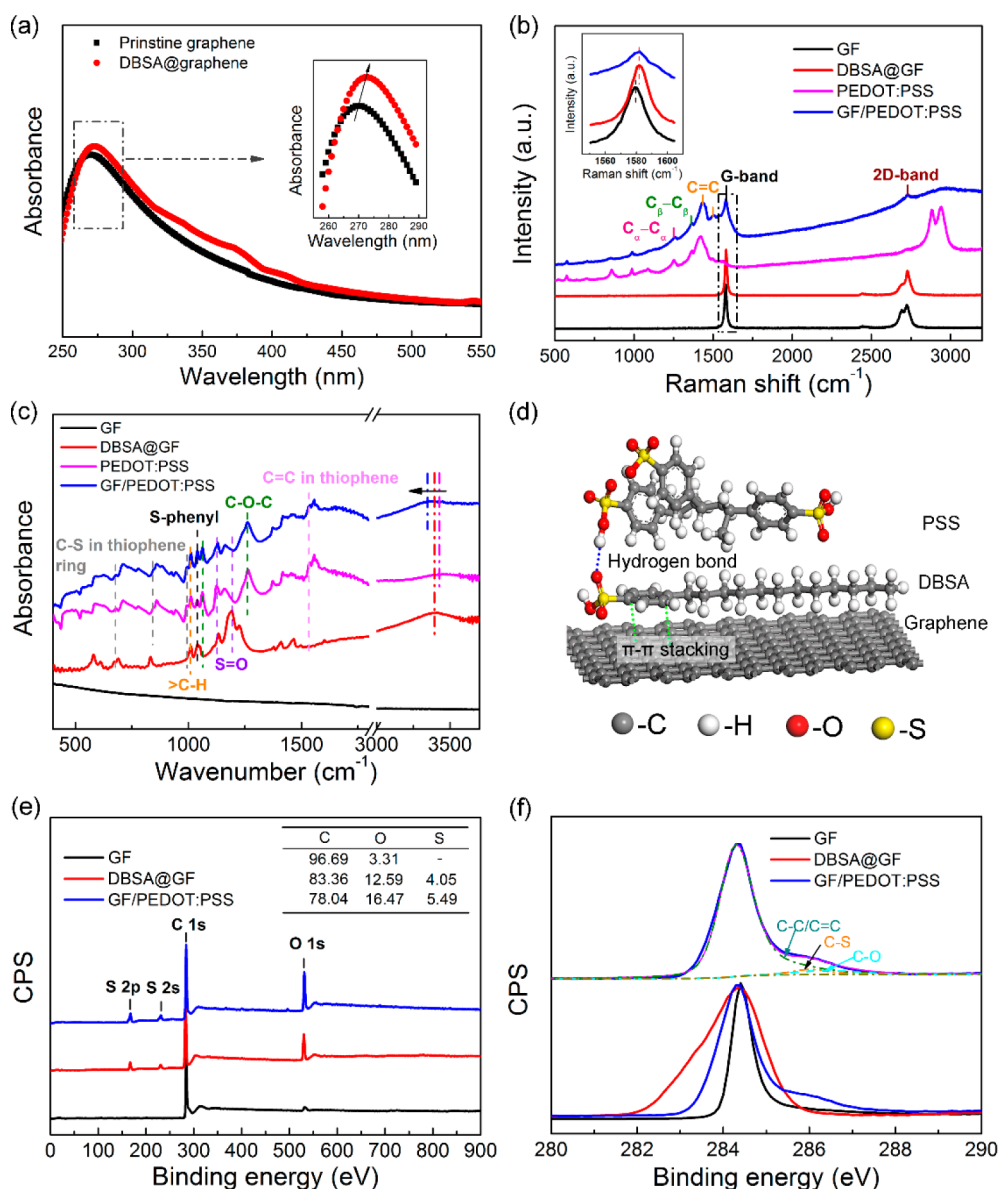


Figure 2. Interfacial interactions among GFs, DBSA and PEDOT:PSS: (a) UV-vis absorption spectra of GFs before and after DBSA treatment; (b) Raman spectra; (c) FT-IR spectra of GFs at different states (insets in (a,b) showing enlarged views of the peaks in the indented regions); (d) schematic illustration of the proposed interfacial interaction mechanisms among graphene, DBSA and PEDOT:PSS (the PEDOT chains being omitted here for simplicity and clearer illustration); and (e) XPS general spectra and (f) deconvoluted C 1s spectra of GF/PEDOT:PSS-0.7 (upper curves).

efficient microwave absorption/shielding capabilities are required.

2. EXPERIMENTAL SECTION

2.1. Synthesis of GFs by CVD Method. Freestanding GFs were produced following the reported procedure, as shown in Figure 1a.^{15,25,26} Ni foams (Heze Tianyu Technology Development) with a thickness of 1.6 mm and an area density of 320 g/m² were cleaned by sonicating in acetone for 90 min, rinsed in deionized (DI) water, and dried in an oven at 60 °C for 24 h. Ni foam templates of 6 cm × 12 cm rectangular shape were put into the quartz tube of a CVD system (OTF-1200X-II-80-SL, Hefei Kejing Materials). After evacuating to 5 mTorr, Ar and H₂ were introduced into the tube at flow rates of 500 standard cubic centimeter per minute (sccm) and 200 sccm, respectively. The furnace was then heated to 1000 °C at a rate of 17 °C/min. The Ni foam substrates were annealed at 1000 °C for 10 min, followed by introducing methane (CH₄) precursor with a concentration of 2.8 vol % for 20 min. After deposition of carbon, the

furnace was quenched to room temperature under Ar and H₂ flows, allowing graphene layers to form on the Ni surface. Freestanding GFs were obtained by etching off the Ni template in a solution of 1 M HCl/0.5 M FeCl₃ at 80 °C. The freestanding GFs were immersed in hot water for 10 min and rinsed with DI water to remove chemical residuals, followed by drying in a vacuum oven at 60 °C overnight. Compressed GFs (CGFs) were fabricated using the identical CVD process for the measurement of contact angles. Four layers of Ni foams of a total thickness of 6.4 mm were compressed to a thickness of 1 mm using a compression jig, which were used as the template for the synthesis of CGFs.

2.2. Fabrication of GF/PEDOT:PSS Composites. Pristine GF was noncovalently functionalized with 4-dodecylbenzenesulfonic acid (DBSA supplied by Aldrich, see Figures S1a,c for its chemical structure) to improve the wettability and enhance the adhesion between GF and PEDOT:PSS. DBSA, an anionic surfactant, was chosen because it is compatible with both graphene and PEDOT:PSS (see Figure S1b for their chemical structures)²⁷ due to the presence of

both hydrophobic tails and hydrophilic heads. The hydrophobic dodecyl group and the benzene ring of DBSA can interact with graphene by adsorption while the sulfo group as its hydrophilic head can interact with the PSS chains. Micelles are formed on graphene surface when the adsorbed DBSA content is at the critical micelle concentration (CMC) (see Figure S 1d for a schematic), and saturation and aggregation occur at a DBSA content above the CMC.²⁸ GFs were immersed in DBSA aqueous solutions with different concentrations for 30 min, followed by rinsing with DI water for several times to remove superfluous DBSA. After drying in a vacuum oven for 12 h, functionalized GFs (DBSA@GF) were obtained. The PEDOT:PSS aqueous solution (CLEVIOS PH 1000) was diluted with the same amount of DI water to reduce its viscosity, followed by addition of 5 vol % dimethyl sulfoxide (DMSO, Sigma-Aldrich, anhydrous). The functionalized GFs were drop coated with the mixture by depositing consecutive drops of different total amounts to obtain different PEDOT:PSS-to-GF mass ratios, which were dried at 80 °C for 0.5 h for evaporation of water and surplus DMSO. The electrical conductivity of the dried PEDOT:PSS film was 850 S/cm. Composites with different PEDOT:PSS contents were fabricated and designated as GF/PEDOT:PSS-X, where X is the mass ratio of PEDOT:PSS to GF.

2.3. Characterization of GF and GF/PEDOT:PSS Composites.

Scanning electron microscope (SEM, JEOL JSM 6390) and transmission electron microscopy (TEM, 2010, JEOL) were used to characterize the morphologies of GFs and GF/PEDOT:PSS composites. The interfacial interactions between the GFs and DBSA were examined by ultraviolet–visible (UV–vis) spectroscopy (PerkinElmer Lambda 20) with a scanning range of 200–800 nm and a quartz chip as the reference. The wettability of functionalized GFs was investigated using the PEDOT:PSS/DMSO solution as the probing liquid on a goniometer (Kruss G10 Contact Angle Measuring System). To avoid the rapid infiltration of probing liquid into the porous GFs during the contact angle measurement, functionalized CGFs with a denser structure (Figure S2) were used. The contact angles were measured after the solution droplets were applied onto the target materials and stabilized for 3 s. Although the contact angles obtained on CGFs were not identical to those measured on ordinary GFs, the trend as a function of DBSA concentration reflected the relative wettability of functionalized GFs. Fourier transform infrared spectroscopy (FT-IR, Bruker Vertex 70 Hyperion 1000) was employed to study the surface chemistry of GFs before and after PEDOT:PSS coating. The crystalline structures of pristine and functionalized GFs and GF/PEDOT:PSS composites were evaluated using the Raman spectroscopy (Reinshaw MicroRaman/Photoluminescence System). X-ray photoelectron spectroscopy (XPS, Axis Ultra DLD) was used to study the chemical elements of functionalized GFs and composites. The electrical conductivities of GFs and GF/PEDOT:PSS composites with different matrix contents were measured using the four-point probe method (Scientific Equipment & Services) with silver paste coating on the contact points. The EMI SEs were calculated from the scattering parameters (S-parameters) which were measured by a waveguide transmission line method using a vector network analyzer (Agilent Technologies N5230A), as shown in Figure S3.²⁹

3. RESULTS AND DISCUSSION

3.1. Characteristics of GFs and GF/PEDOT:PSS Composites. The morphologies of freestanding GFs (Figure 1b,c) are essentially similar to those obtained previously,^{15,26} which possessed a cellular porous structure with wrinkles on the surface arising from the grain boundaries of the underlying Ni foam templates. The GFs fabricated in this study were composed of ~12 layers of graphene on average (inset in Figure 1c), which is consistent with previous studies.^{25,26} The as-prepared GFs was highly hydrophobic due to the absence of oxygen-containing functional groups, making it incompatible with the PEDOT:PSS aqueous solution. After functionalization, however, GFs became reactive and were uniformly coated with

PEDOT:PSS (Figure 1d). The contact angle of GFs decreased with increase in surfactant concentration, signifying enhanced wettability and physical interactions with the PEDOT:PSS coating (Figure 1e). One of the major benefits of noncovalent functionalization using a surfactant compared to covalent functionalization, such as oxidation,³⁰ amination,³¹ and silanation,³² is that the graphene's hexagonal structure remains intact²⁸ so that its inherent electrical conductivity is not adversely affected. The pristine GF presented a very low wettability with a large contact angle of 113° (inset 1), resulting in detachment of polymer coating upon application. After functionalization with a low concentration DBSA solution, the contact angle decreased with enhanced wettability (inset 2), although the PEDOT:PSS solution was still unable to penetrate into the internal space. The functionalized GF by 0.75 wt % DBSA allowed uniform coating of PEDOT:PSS solution (inset 3). With higher DBSA concentrations, however, the contact angle decreased only marginally probably due to these DBSA concentration approaching its CMC. In view of the insulating nature of DBSA surfactant, the concentration of 0.75 wt % was chosen for composite fabrication to balance the electrical conductivity and the interfacial bond.

The enhanced interfacial bonds between GF and PEDOT:PSS were confirmed by the UV–vis, Raman, FT-IR spectra, and XPS spectra, as shown in Figure 2. The obvious UV–vis absorption peak located at 269 nm is a reflection of phenyl groups³³ of pristine GF (Figure 2a). Upon functionalization, the peak position up-shifted to 271 nm, suggesting π – π stacking interactions between the benzene rings of graphene and DBSA.³³ Theoretical calculations demonstrate that the π – π interactions take place only when the intermolecular distance is about 3–4 Å,³⁴ meaning that it is rather difficult to form π – π interactions between different species without external forces. However, the very short molecular chains of DBSA made the stacking possible, which may also explain the relatively small upshift of the peak position compared with reported data.³³ The Raman spectrum of pristine GFs (Figure 2b) presents G- and 2D-band peaks centered at ~1580 and ~2700 cm^{-1} , respectively. The D-band at ~1350 cm^{-1} , a reflection of sp^3 hybridization, was absent in the as-prepared GFs because of the perfect graphitic structure with negligible defects. The 2D peak at ~2700 cm^{-1} was split into two small peaks, indicating that multilayered graphene sheets (Figure 1c) were grown during the CVD process.³⁵ The PEDOT:PSS matrix exhibited a prominent peak at 1430 cm^{-1} , which is attributed to the symmetric stretching vibration of the aromatic C=C bond.⁴ The peak at ~1506 cm^{-1} is a representative of the asymmetric stretching vibrations of thiophene rings in the middle of PEDOT chains.³⁶ The peaks at 1259 and 1361 cm^{-1} are assigned to the C_α - C_α and C_β - C_β stretching deformation in PEDOT:PSS,⁴ respectively. The GF/PEDOT:PSS composite exhibited characteristic peaks of both GF and PEDOT:PSS, suggesting strong adhesion of polymer coating onto the GF. The G-band of pristine GF upshifted from 1579 to 1582 cm^{-1} (inset of Figure 2b) after the functionalization, confirming the formation of π – π stacking between GFs and DBSA.³⁷ However, the G-band position presented no further increment after the coating of PEDOT:PSS (Figure S4), indicative of a negligible doping effect of PEDOT:PSS on GFs. It appears that the presence of DBSA molecular layers on GFs impeded the direct contact between graphene and PEDOT:PSS, making the doping of graphene rather difficult.

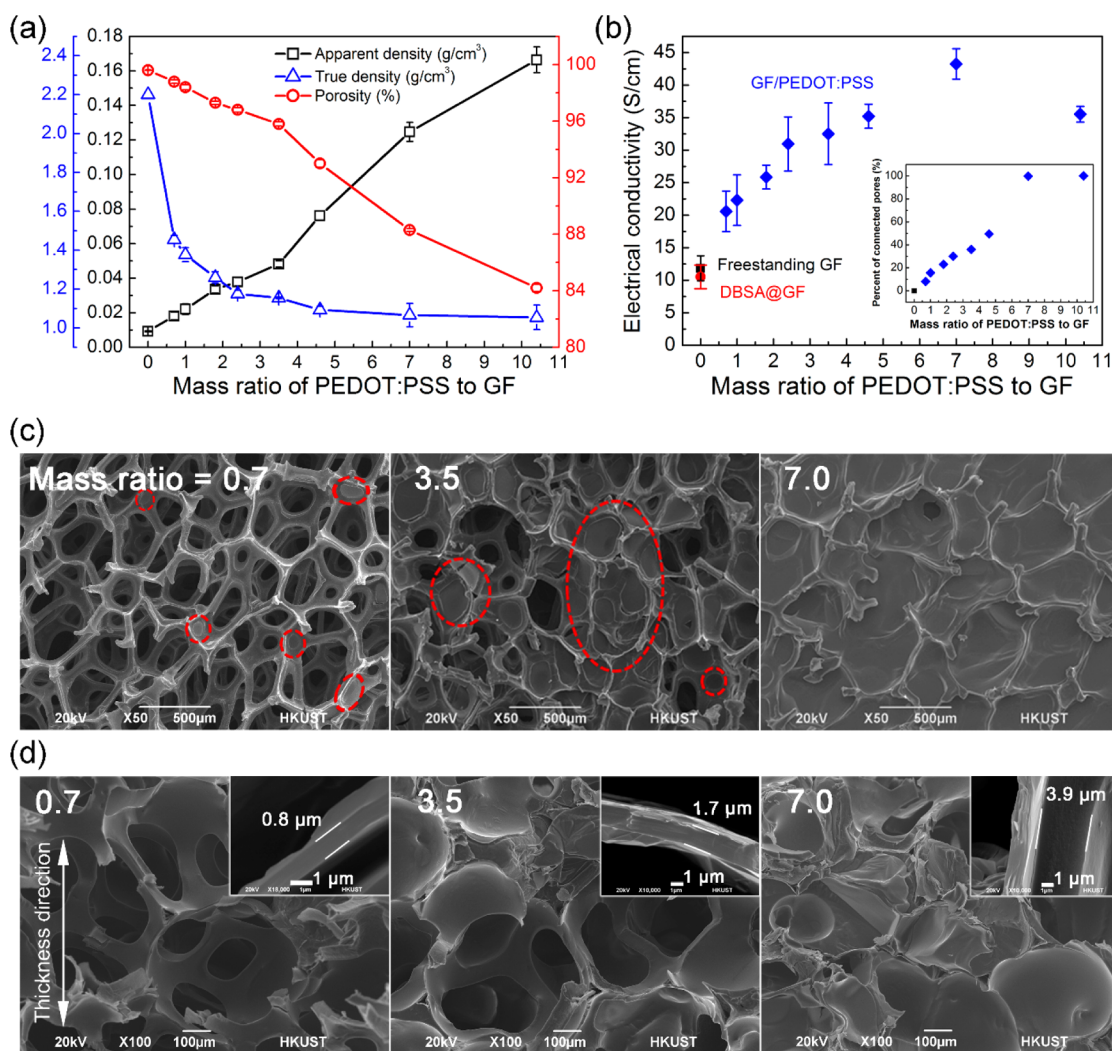


Figure 3. (a) Densities and porosities and (b) electrical conductivities of GF/PEDOT:PSS composites as a function of mass ratio of PEDOT:PSS to GFs with percent of connected pores in inset; SEM images of (c) surface and (d) cross sections of freeze-fractured GF/PEDOT:PSS composites with different mass ratios. Red circles in (c) indicate connected pores by the PEDOT:PSS films. Insets in (d) show the thicknesses of the conductive polymer coating layers.

There was no peak observed in the FT-IR spectrum of pristine GFs due to the absence of functional groups (Figure 2c). After the functionalization of GFs, characteristic peaks of DBSA appeared: namely, > C–H vibration located at 1007 cm⁻¹, S-phenyl bonds at 1037 cm⁻¹ and two S–O bonds at 1123 and 1187 cm⁻¹.³⁸ It is noted that PEDOT:PSS showed different peaks from those of DBSA, including C–S bonds in thiophene ring at 680, 844, and 991 cm⁻¹, C–O–C stretching peaks at 1065 and 1260 cm⁻¹, and C=C stretching vibrations of the thiophene ring at 1522 cm⁻¹.³⁸ The broad band at ~3400 cm⁻¹ is associated with the stretching vibration of O–H bonds.³⁷ It was very weak in PEDOT:PSS probably because of the steric hindrance caused by the large benzene rings in PSS chains, making the O–H groups difficult to interact with each other. However, the O–H peak became more obvious in the GF/PEDOT:PSS composite because of the large amount of O–H groups in DBSA. Moreover, the peak position downshifted after the formation of GF/PEDOT:PSS composite, an indication of hydrogen bonds between DBSA and the PSS chains.³⁹ Based on the above findings, we can conclude that DBSA is a very effective surfactant for improving both the wettability and interactions between the pristine GF and

PEDOT:PSS matrix by forming π – π stacking with graphene and hydrogen bonds with PSS chains. The mechanism of enhanced interfacial bonds between graphene, DBSA and PEDOT:PSS is schematically illustrated in Figure 2d. The general XPS spectrum of freestanding GFs (Figure 2e) exhibited a dominant C 1s peak and a weak O 1s peak, the latter being a reflection of the moisture adsorbed on the GF surface from the atmosphere. An obvious S 2p peak and a significantly enhanced O 1s peak in the DBSA functionalized GFs and the GF/PEDOT:PSS composite were also noted. After the DBSA treatment, the deconvoluted C 1s spectrum became much broader than that of the pristine GFs or the GF/PEDOT:PSS composite (Figure 2f), a testament to strong interfacial bonds between DBSA and GFs.⁴⁰ The C 1s of the GF/PEDOT:PSS composite (upper spectrum in Figure 2f) consisted of three functional groups, including C=C/C–C (284.4 eV), C–S (286.1 eV), and C–O–C (286.5 eV) groups.³⁹ The elemental compositions of GFs, DBSA@GF, GF/PEDOT:PSS were analyzed (see inset of Figure 2e) and summarized in Table S1. Both C–S and C–O–C were absent on the pristine GFs, while a small amount of C–S bonds (~4.6%) appeared on the functionalized GFs arising from the

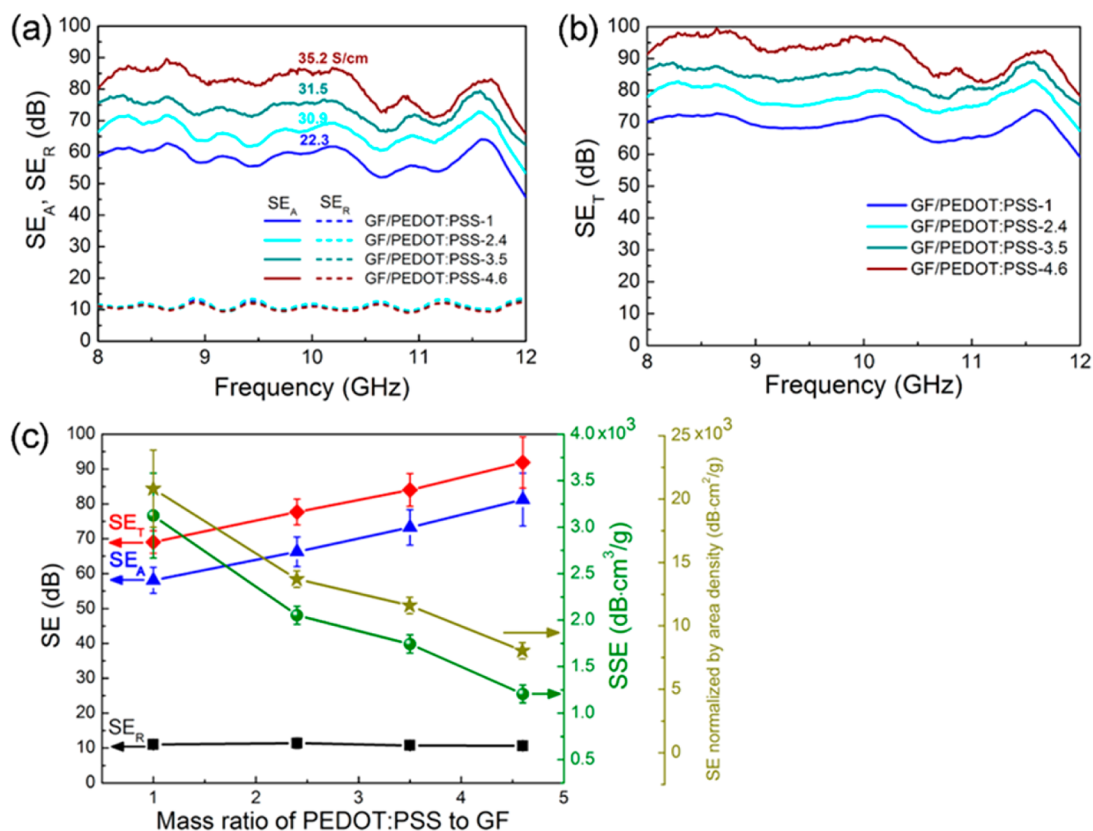


Figure 4. EMI SEs of composites with different compositions: (a) SEA and SER, (b) SET as a function frequency; and (c) summary of SEs, SSEs, and SSEs normalized by area density as a function of mass ratio of PEDOT:PSS to GF.

thin layer of DBSA molecules on GFs. After the incorporation of PEDOT:PSS coating, C–O–C appeared as a characteristic peak of PSS chains.

3.2. Densities and Electrical Conductivities of Composites. The porosities (β) of GF/PEDOT:PSS composites with different polymer to graphene mass ratios were calculated using the following equation:⁴¹

$$\beta = (1 - \rho_a/\rho_t) \times 100\% \quad (1)$$

where ρ_a is the apparent density determined by the ratio of total mass to volume of materials and ρ_t represents the true density depending on the masses and densities of different components according to eq 2:

$$\rho_t = \frac{m_C}{m_G \rho_G^{-1} + m_P \rho_P^{-1}} \quad (2)$$

where m is the mass and the subscripts C, G, and P refer to the composite, graphene, and PEDOT:PSS, respectively. The densities of graphene³⁹ and PEDOT:PSS are 2.2 and 1 g/cm³ (according to the supplier's specification), respectively. The true densities and porosities of the composites with different PEDOT:PSS-to-GF mass ratios are plotted in Figure 3a. The pristine freestanding GF possessed a low apparent density of 9.29×10^{-3} g/cm³ and a high porosity of 99.6%. With increasing polymer content, the true density of composites initially decreased rapidly followed by slow reductions while the apparent density increased almost linearly. As expected, the porosity was roughly inversely proportional to the apparent density.

As shown in Figure 3b, the electrical conductivity of the GF/PEDOT:PSS composite gradually increased with increasing

conducting polymer content, reaching a peak of 43.2 S/cm at a PEDOT:PSS-to-GF mass ratio of ~ 7 , followed by saturation afterward. As discussed above, the potential doping effect of PEDOT:PSS on conductivity of graphene was almost absent in this study because of the steric hindrance caused by the DBSA molecules applied on GFs. The enhanced electrical conductivities of the GF/PEDOT:PSS composite are attributed mainly to the enhanced conducting networks. The PEDOT:PSS coating with a high electrical conductivity of 850 S/cm had major ameliorating effects on both the microscopic and nanoscopic scales. (i) The microscopic effect arose from the gradual changes in porous structure of the composites with different polymer contents. Figure 3c shows that the large openings—both internal and external—present between the skeleton of cellular GFs were connected by the conductive PEDOT:PSS, leading to enhanced conductive networks. The interconnected structure with large cellular pores and the excellent wettability of functionalized GFs allowed the diluted PEDOT:PSS aqueous solution with a low viscosity to infiltrate into the inside of GFs via a step-by-step drop-coating. Both the surface and the center of GFs were effectively coated by PEDOT:PSS, as shown in Figure 3c,d. The thicknesses of the polymer coating layers on graphene tubes increased gradually from ~ 0.8 to $3.9 \mu\text{m}$ when the PEDOT:PSS-to-GF mass ratio was increased from 0.7 to 7 (insets of Figure 3d). It is obvious that the number of pores connected by PEDOT:PSS increased with increasing polymer content: an increase in polymer to GF mass ratio from 3.5 to 7.0 resulted in a surge in percentage of interconnected surface pores from $\sim 36\%$ to almost 100%, reaching the peak electrical conductivity (Figure 3b). However, once all pores were covered, the conductivity enhancement by

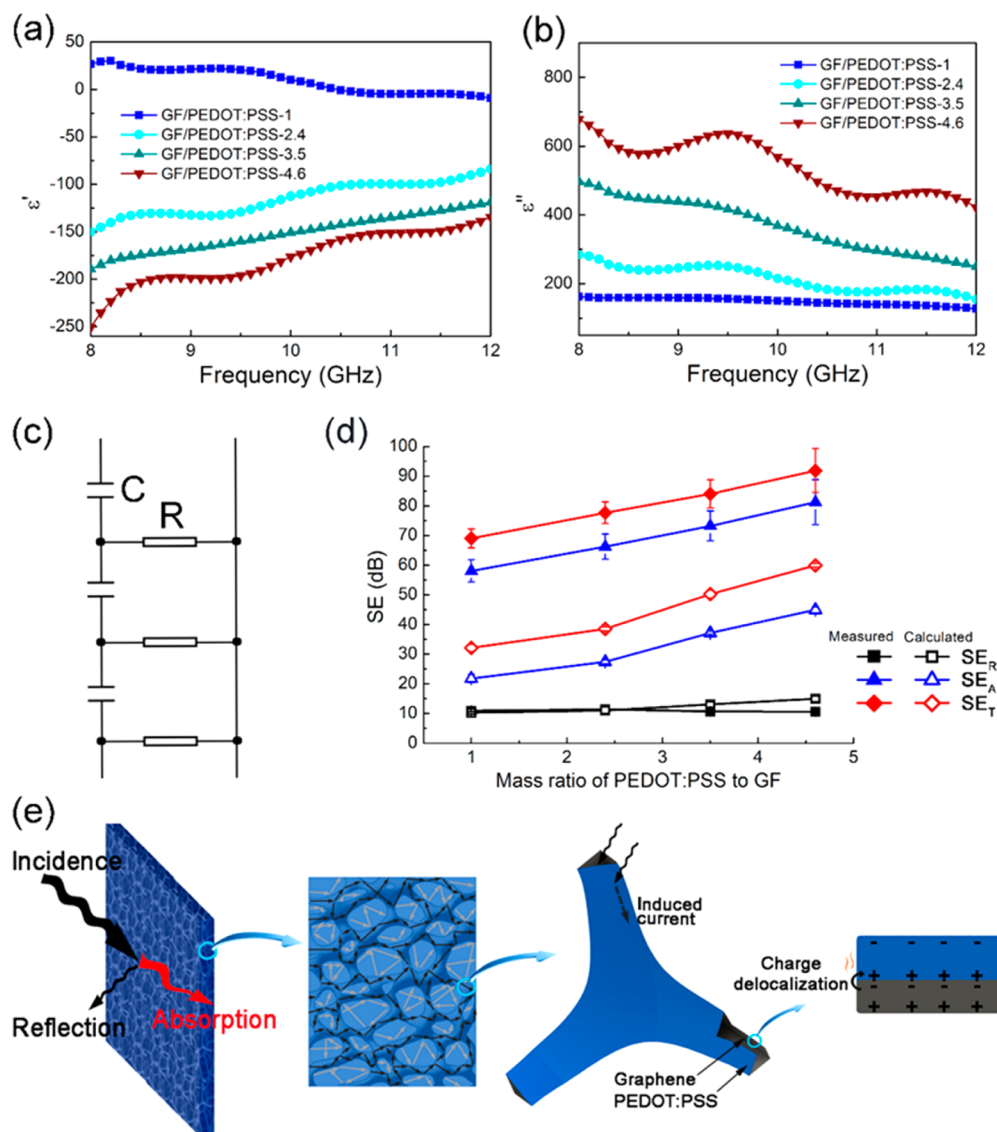


Figure 5. (a) Real and (b) imaginary parts of permittivity of composites with different mass ratios of PEDOT:PSS to GF; (c) the equivalent circuit model of left-handed composites; (d) comparison of experimental and theoretical EMI SEs of different composites; and (e) schematic illustration of EMI shielding mechanisms.

increasing the polymer content became difficult due to saturation. (ii) The nanoscopic effect refers the enhanced conductivity when the PEDOT:PSS coating served as the conducting bridges across the resistive grain boundaries in GFs, as shown in Figure 1c,d.

3.3. EMI Shielding Properties. There are three main mechanisms responsible for EMI shielding of a material, including reflection, absorption attenuation, and multiple reflection of EM waves.⁴² Since the reflection of EM radiations is a result of the interactions between the EM waves and free charges on the surface of materials, electrically conductive networks with a large amount of charge carriers are beneficial to EMI shielding effectiveness by reflection, SE_R .⁴³ The absorption is a measure of the capacity of materials to attenuate EM energies into thermal and/or internal energies. Any types of energy dissipation and energy consuming responses induced by EM radiations, such as localized currents generated in conductive networks and polarization/relaxation processes of dipoles and free charges, contribute to the absorption effectiveness, SE_A , of materials.⁴³ When the SE_A is higher

than 10 dB, most of the multiply reflected waves can be further absorbed. Therefore, the EMI SE_A of polymer-based composites reinforced by conductive fillers is attributed to both direct absorption and the absorption of multiply reflected radiations.²¹ Thus, the reflection and absorption are dominant mechanisms of the 3D graphene/polymer composites with which this work is mainly concerned.

The total EMI SE, SE_T , is the logarithm of the power ratio of incident EM waves, P_I to transmitted wave, P_T , measured by the S-parameters, S_{11} and S_{21} :⁵

$$SE_T = 10\log(P_I/P_T) \quad (3)$$

$$|S_{11}| = \sqrt{P_R/P_I} \quad (4)$$

$$|S_{21}| = \sqrt{P_T/P_I} \quad (5)$$

where P_R refers to the power of reflected wave. The reflection coefficient, R , transmission coefficient, T , and absorption coefficient, A , can be calculated using eqs 6–8:¹⁵

$$R = |S_{11}|^2 \quad (6)$$

$$T = |S_{21}|^2 \quad (7)$$

$$A = 1 - R - T \quad (8)$$

The SE values contributed by reflection, SE_R , absorption, SE_A , and the total SE, SE_T , of materials are determined by

$$SE_R(\text{dB}) = -10\log(1 - R) \quad (9)$$

$$SE_A(\text{dB}) = -10\log[T/(1 - R)] \quad (10)$$

$$SE_T(\text{dB}) = SE_R + SE_A \quad (11)$$

The EMI shielding performance of the composites with different PEDOT:PSS-to-GF mass ratios is plotted for frequency range of 8–12 GHz, as shown in Figure 4. When the mass ratio increased from 1 to 4.6, SE_A showed a continuous increase while SE_R maintained a negligible change at low values fluctuating between 9 and 13 dB (Figure 4a). The GF/PEDOT:PSS-1 composite with an electrical conductivity of 22.3 S/cm exhibited an average SE_T of 69.1 dB, whereas the GF/PEDOT:PSS-4.6 composite with a higher electrical conductivity of 35.2 S/cm had a higher average SE_T of 91.9 dB (Figure 4b,c). The SE_A and SE_R were analyzed to identify predominant EMI shielding mechanisms for the composites. It is noticed that SE_A contributes more than 80% of the total SE_T for all composites studied, indicating that the attenuation of microwave energies into thermal/internal energies was dominant. However, the contribution by SE_R to the total SE_T was very limited.

Possessing very low apparent densities ranging from 0.0221 to 0.0762 g/cm³ corresponding to the mass ratios ranging from 1 to 4.6, the GF/PEDOT:PSS composites delivered extremely high SSEs determined by normalizing the SE_T by the composite density (Figure 4c). An extraordinarily high SSE of 3124 dB·cm³/g was achieved for GF/PEDOT:PSS-1 due to its high SE_T with a low density. With increasing density, the SSEs suffered, showing a lower SSE of 1206 dB·cm³/g for GF/PEDOT:PSS-4.6. The thickness of material is another important parameter that determines the EMI shielding performance. With a constant thickness of 1.5 mm, the GF/PEDOT:PSS composites possessed SEs normalized by area density ranging from 8040 to 20 800 dB·cm²/g (Figure 4c).

In order to understand the mechanisms responsible for the much enhanced EMI shielding performances of GF/PEDOT:PSS composites, their permittivity and permeability were specifically studied. Upon exposure of the composite to EM waves, polarization occurs in two sources: namely, interfacial polarization owing to different electrical conductivities of GF and PEDOT:PSS, and dipolar polarization in the PEDOT:PSS chains. It is observed that the absolute value of the real part of permittivity, ϵ' , increases with increasing polymer content (Figure 5a) due to the enhanced dipolar polarization. The majority of composites consisting of conductive fillers and insulating polymer matrices were reported to possess positive permittivities because of the interfacial polarization arising from the difference in electrical conductivities of fillers and matrices. On the contrary, negative permittivity (Figure 5a) and permeability values (Figure S5b) were obtained for the present GF/PEDOT:PSS composites, which were also reported previously for conductive polymer composites with strong interfacial interactions and continuous conductive networks.^{44–47} With three-dimensionally intercon-

nected conductive networks of GFs and a highly conductive PEDOT:PSS coating, the polarized charge was delocalized macroscopically instead of being aggregated at the interfaces, leading to the negative permittivity.^{44,45,48} Within the frequency range of 8–12 GHz, the wavelengths, λ , of the incident radiation were in the range of 25–37.5 mm, which are much longer than the diameter of graphene tubes in GFs (Figure 1b,c). λ was determined by $\lambda = cf^{-1}$, where c and f are the light velocity and the frequency, respectively. As a result, resonance can occur in the composites, leading to negative permittivities.⁴⁹ The refractive index (n) given by $n = \pm\sqrt{\epsilon\mu}$ is related to the sign of the permittivity (ϵ) and permeability (μ). With negative values of both parameters, the refractive index is negative for the GF/PEDOT:PSS composites, which can be defined as the left-handed material.⁵⁰ It is well-known that the EM waves cannot propagate inside a lossy left-handed material with its absolute permittivity and/or permeability larger than 1.⁵⁰ In other words, waves are effectively attenuated or absorbed, giving rise to a high EMI SE_A with few transmitted waves. Therefore, it can be concluded that the excellent EMI shielding performance of GF/PEDOT:PSS is attributed to both the capacitor-like behavior induced by polarization and resistor-like characteristics originating from the highly conductive composite networks, showing a left-handed equivalent circuit character as schematically shown in Figure 5c.⁵¹ The charge delocalization in the highly conductive network has contributed as well. The localized eddy current generated by alternating EM fields¹⁵ can also be easily dissipated by fully connected conductive networks (Figure 5e).

Once the electrical conductivity, σ , of composites satisfies $\sigma = \sigma_{ac} + \sigma_{dc} \gg 2\pi f\epsilon_0$ (where σ_{ac} , σ_{dc} and $\epsilon_0 = 8.854 \times 10^{-12}$ F/m are the alternating current conductivity, the direct current conductivity and the vacuum permittivity, respectively), the shielding effectiveness values, SE_A and SE_R , can be theoretically estimated by the following equations which are usually applied to solid conductive materials:^{52,53}

$$SE_R = 10\log\left(\frac{\sigma_{ac}}{32\pi f\epsilon_0\mu'}\right) \quad (12)$$

$$SE_A = 8.68t\sqrt{\sigma_{ac}\pi f\mu_0\mu'} \quad (13)$$

where μ_0 ($= 1.257 \times 10^{-6}$ H/m), μ' , and t are the vacuum permeability, the real permeability, and the sample thickness, respectively. The alternative current conductivity is determined by $\sigma_{ac} = 2\pi f\epsilon_0\epsilon''$, where ϵ'' is the imaginary permittivity. Because the electrical conductivity of over 20 S/cm of the GF/PEDOT:PSS composite was much higher than the largest value of $2\pi f\epsilon_0$ (0.67 Hz F/m) in the frequency range of 8–12 GHz, both SE_A and SE_R were determined by the permittivity, permeability, and electrical conductivity. Figure 5d presents the comparison of SE_R , SE_A , and SE_T between the calculation and experimental data. As described in the above, the reflection of EM waves, SE_R , is mainly attributed to the interactions between radiations and free charges on the surface, while the morphological features of material such as porosity and cellularity have a negligible effect.⁴³ Therefore, the calculation and experiment agree very well for SE_R . However, the calculated SE_A values were always lower, by over 35 dB, than the measured values because that eq 13 only takes material properties—electrical conductivity, permittivity, and permeability—into account, while the material morphologies are also related to SE_A . It has been confirmed that porous structures are

beneficial for EMI shielding. For example, an enhanced SE_A was obtained by foaming of graphene sheets despite the lower electrical conductivity, while SE_R showed little change.¹¹ Multiple reflections within and between the hollow graphene tubes of GFs enhanced interactions between the shielding material and EM waves. Charge delocalization between GF and the PEDOT:PSS coating which is not taken into account in eq 13 is another significant contribution to SE_A , as summarized in Figure 5e.

To verify the benefits of using lightweight composites for EMI shielding, a comprehensive comparison was performed between the GF/PEDOT:PSS composites and other nanocarbon-based composites with relatively low densities ($<1.2 \text{ g/cm}^3$), as shown in Figure 6. The details of their EMI SEs and

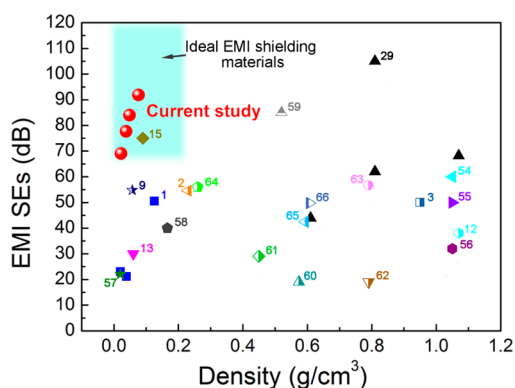


Figure 6. Comparison of EMI SEs of different carbon-based materials as a function of density of materials: multiwall CNT (MWCNT)/waterborne polyurethane (WPU) aerogels;¹ CuNi/CNT foam;² graphene oxide/cellulose aerogels;⁹ aligned rGO/epoxy;¹² porous GF/PDMS;¹³ porous CNT/GF/PDMS;¹⁵ graphene papers;²⁹ MWCNT/PS;⁵⁴ MWCNT/acrylonitrile-butadiene-styrene;⁵⁵ graphene/WPU;⁵⁶ CNT sponge;³⁷ commercial carbon foam;⁵⁸ MWCNTs decorated carbon foam;⁵⁹ CNT/PS foam;⁶⁰ porous graphene/PS;⁶¹ graphene/poly(methyl methacrylate) foam;⁶² porous MWCNT/PVDF;⁶³ MWCNT-based mesocarbon microbead composite paper;⁶⁴ silicon carbide nanowires/carbon foam;⁶⁵ carbon foams.⁶⁶

physical properties are given in Table S2. For solid polymer-based composites reinforced with conductive fillers, the reported EMI SEs varied in the range of 20–60 dB.^{12,54–56} The SSEs of solid CPCs having relatively high densities over 0.8 g/cm^3 are very low. Graphene papers fabricated by CVD growth on a Ni template showed a high EMI SEs of over 100 dB,²⁹ but their SSEs were low because of their high densities. Porous materials, such as carbon foams^{57–59} and CPC foams,^{1,9,13,60,61} have densities of generally lower than 0.5 g/cm^3 . With comparable SEs of 20–60 dB, these porous systems can outperform the solid CPCs in terms of SSE, although their morphologies are not fully optimized and they have limited electrical conductivities. The GF/PEDOT:PSS composites in this study presented extremely high EMI SEs of 65–91.9 dB at ultralow densities of $0.022\text{--}0.076 \text{ g/cm}^3$. The extremely low densities of the GF/PEDOT:PSS composites with high EMI SEs place them among the ideal EMI shielding materials especially for applications where lightweight is an important criterion, such as portable electronics and aerospace structures.

4. CONCLUSION

This paper reports a new strategy for the fabrication of GF/PEDOT:PSS composites with different PEDOT:PSS-to-GF

mass ratios. Freestanding GFs were synthesized by CVD on Ni templates and functionalized with DBSA, on which the PEDOT:PSS aqueous solution was applied to form a coating with uniform thickness. The resulting interconnected, highly conductive GF/PEDOT:PSS composites showed exceptional EMI shielding properties. The following can be highlighted from the experimental and theoretical studies:

(i) The CVD-grown, cellular-structured, freestanding GFs had an extremely low density of $9.3 \times 10^{-3} \text{ g/cm}^3$ and a porosity of 99.6%. The GFs were functionalized using DBSA surfactant, which effectively enhanced the wettability and interfacial adhesion between GFs and PEDOT:PSS to form uniformly coated composites. The $\pi\text{--}\pi$ stacking between GFs and DBSA and the hydrogen bonds between PEDOT:PSS and DBSA were responsible for the enhanced interfacial interactions between the composite constituents.

(ii) The apparent densities of composites gradually increased from 0.0182 to 0.1664 g/cm^3 while the porosities showed a gradual decrease from 98.8 to 84.2% as the PEDOT:PSS-to-GF mass ratio was increased from 0.7 to 11.4. These physical/morphological changes gave rise to a modification of electrical conductivities of GF/PEDOT:PSS composites, reaching a peak value of 43.2 S/cm at a mass ratio of 7.0. The PEDOT:PSS coating with a high conductivity of 850 S/cm had two ameliorating effects on composite electrical conductivity, namely the connection of large openings among the cellular graphene skeleton on a microscopic scale and bridging across the resistive grain boundaries of GFs on a nanoscopic scale to form consolidated conducting networks.

(iii) The optimized GF/PEDOT:PSS composites delivered exceptional EMI SEs, with a largest value of 91.9 dB. Owing to their extremely low densities, the composites possessed even more remarkable SSEs in the ranges of 1206–3124 and 8040–20 800 $\text{dB}\cdot\text{cm}^2/\text{g}$, when normalized by volumetric and area densities, respectively. These SSE values are the highest among similar composites containing nanocarbon fillers. The high conductivities of the composite arising from both the GFs with inherent conductive networks and the conductive polymer coating, the porous structure, and the effective charge delocalization were mainly responsible for the predominant contribution to microwave attenuation by absorption, SE_A .

■ ASSOCIATED CONTENT

Supporting Information

The Supporting Information is available free of charge on the ACS Publications website at DOI: 10.1021/acsami.7b01017.

Chemical structures, schematics of the EMI measurement setup, Raman spectra and the permeability of composites, summary of carbon bonds of different materials and comparison data table (PDF)

■ AUTHOR INFORMATION

Corresponding Authors

*E-mail: mezheng@ust.hk.

*E-mail: mejkkim@ust.hk.

ORCID

Xi Shen: 0000-0003-1688-4931

Jang-Kyo Kim: 0000-0002-5390-8763

Notes

The authors declare no competing financial interest.

ACKNOWLEDGMENTS

This project was financially supported by the Research Grants Council of Hong Kong SAR (GRF Projects: 16203415 and 16229216). Y.W. and X.L. were supported by the Postgraduate Scholarship of HKUST. Z.W. and X.S. were recipients of the Hong Kong Ph.D. Fellowship. Technical assistance from the Materials Characterization and Preparation Facilities (MCPF) and the Advanced Engineering Material Facility (AEMF) at HKUST is also appreciated.

REFERENCES

- (1) Zeng, Z.; Jin, H.; Chen, M.; Li, W.; Zhou, L.; Zhang, Z. Lightweight and Anisotropic Porous MWCNT/WPU Composites for Ultrahigh Performance Electromagnetic Interference Shielding. *Adv. Funct. Mater.* **2016**, *26*, 303–310.
- (2) Ji, K.; Zhao, H.; Zhang, J.; Chen, J.; Dai, Z. Fabrication and Electromagnetic Interference Shielding Performance of Open-cell Foam of A Cu–Ni Alloy Integrated with CNTs. *Appl. Surf. Sci.* **2014**, *311*, 351–356.
- (3) Im, J. S.; Kim, J. G.; Lee, Y.-S. Fluorination Effects of Carbon Black Additives for Electrical Properties and EMI Shielding Efficiency by Improved Dispersion and Adhesion. *Carbon* **2009**, *47*, 2640–2647.
- (4) Nguyen, T. P.; Le Rendu, P.; Long, P. D.; De Vos, S. A. Chemical and Thermal Treatment of PEDOT:PSS Thin Films for Use in Organic Light Emitting Diodes. *Surf. Coat. Technol.* **2004**, *180*, 646–649.
- (5) Cao, M.-S.; Song, W.-L.; Hou, Z.-L.; Wen, B.; Yuan, J. The Effects of Temperature and Frequency on the Dielectric Properties, Electromagnetic Interference Shielding and Microwave-Absorption of Short Carbon Fiber/Silica Composites. *Carbon* **2010**, *48*, 788–796.
- (6) Goyal, R. K.; Kadam, A. Polyphenylene Sulphide/Graphite Composites for EMI Shielding Applications. *Adv. Mater. Lett.* **2010**, *1*, 143–147.
- (7) Geetha, S.; Sathesh Kumar, K. K.; Rao, C. R. K.; Vijayan, M.; Trivedi, D. C. EMI Shielding: Methods and Materials—A Review. *J. Appl. Polym. Sci.* **2009**, *112*, 2073–2086.
- (8) Kuang, T.; Chang, L.; Chen, F.; Sheng, Y.; Fu, D.; Peng, X. Facile Preparation of Lightweight High-Strength Biodegradable Polymer/Multi-Walled Carbon Nanotubes Nanocomposite Foams for Electromagnetic Interference Shielding. *Carbon* **2016**, *105*, 305–313.
- (9) Wan, C.; Li, J. Graphene Oxide/Cellulose Aerogels Nanocomposite: Preparation, Pyrolysis, and Application for Electromagnetic Interference Shielding. *Carbohydr. Polym.* **2016**, *150*, 172–179.
- (10) Li, X.-H.; Li, X.; Liao, K.-N.; Min, P.; Liu, T.; Dasari, A.; Yu, Z.-Z. Thermally Annealed Anisotropic Graphene Aerogels and Their Electrically Conductive Epoxy Composites with Excellent Electromagnetic Interference Shielding Efficiencies. *ACS Appl. Mater. Interfaces* **2016**, *8*, 33230–33239.
- (11) Shen, B.; Li, Y.; Yi, D.; Zhai, W.; Wei, X.; Zheng, W. Microcellular Graphene Foam for Improved Broadband Electromagnetic Interference Shielding. *Carbon* **2016**, *102*, 154–160.
- (12) Yousefi, N.; Sun, X.; Lin, X.; Shen, X.; Jia, J.; Zhang, B.; Tang, B.; Chan, M.; Kim, J.-K. Highly Aligned Graphene/Polymer Nanocomposites with Excellent Dielectric Properties for High-performance Electromagnetic Interference Shielding. *Adv. Mater.* **2014**, *26*, 5480–5487.
- (13) Chen, Z.; Xu, C.; Ma, C.; Ren, W.; Cheng, H.-M. Lightweight and Flexible Graphene Foam Composites for High-Performance Electromagnetic Interference Shielding. *Adv. Mater.* **2013**, *25*, 1296–1300.
- (14) Chen, Y.; Zhang, H.-B.; Yang, Y.; Wang, M.; Cao, A.; Yu, Z.-Z. High-Performance Epoxy Nanocomposites Reinforced with Three-Dimensional Carbon Nanotube Sponge for Electromagnetic Interference Shielding. *Adv. Funct. Mater.* **2016**, *26*, 447–455.
- (15) Sun, X.; Liu, X.; Shen, X.; Wu, Y.; Wang, Z.; Kim, J.-K. Graphene Foam/Carbon Nanotube/Poly(dimethyl siloxane) Composites for Exceptional Microwave Shielding. *Composites, Part A* **2016**, *85*, 199–206.
- (16) Singh, A. P.; Mishra, M.; Hashim, D. P.; Narayanan, T.; Hahm, M. G.; Kumar, P.; Dwivedi, J.; Kedawat, G.; Gupta, A.; Singh, B. P. Probing the Engineered Sandwich Network of Vertically Aligned Carbon Nanotube–Reduced Graphene Oxide Composites for High Performance Electromagnetic Interference Shielding Applications. *Carbon* **2015**, *85*, 79–88.
- (17) Kumar, R.; Kumari, S.; Dhakate, S. R. Nickel Nanoparticles Embedded in Carbon Foam for Improving Electromagnetic Shielding Effectiveness. *Appl. Nanosci.* **2015**, *5*, 553–561.
- (18) Chen, Y.; Wang, Y.; Zhang, H.-B.; Li, X.; Gui, C.-X.; Yu, Z.-Z. Enhanced Electromagnetic Interference Shielding Efficiency of Polystyrene/Graphene Composites with Magnetic Fe₃O₄ Nanoparticles. *Carbon* **2015**, *82*, 67–76.
- (19) Chen, Y.; Zhang, H.-B.; Huang, Y.; Jiang, Y.; Zheng, W.-G.; Yu, Z.-Z. Magnetic and Electrically Conductive Epoxy/Graphene/Carbon-nyl Iron Nanocomposites for Efficient Electromagnetic Interference Shielding. *Compos. Sci. Technol.* **2015**, *118*, 178–185.
- (20) Liu, P.-B.; Huang, Y.; Sun, X. Excellent Electromagnetic Absorption Properties of Poly(3, 4-ethylenedioxythiophene)-Reduced Graphene Oxide–Co₃O₄ Composites Prepared by A Hydrothermal Method. *ACS Appl. Mater. Interfaces* **2013**, *5*, 12355–12360.
- (21) Zeng, Z.; Chen, M.; Jin, H.; Li, W.; Xue, X.; Zhou, L.; Pei, Y.; Zhang, H.; Zhang, Z. Thin and Flexible Multi-Walled Carbon Nanotube/Waterborne Polyurethane Composites with High-Performance Electromagnetic Interference Shielding. *Carbon* **2016**, *96*, 768–777.
- (22) Saini, P.; Choudhary, V.; Singh, B.; Mathur, R.; Dhawan, S. Enhanced Microwave Absorption Behavior of Polyaniline-CNT/Polystyrene Blend in 12.4–18.0 GHz Range. *Synth. Met.* **2011**, *161*, 1522–1526.
- (23) Kim, M.; Kim, H.; Byun, S.; Jeong, S.; Hong, Y.; Joo, J.; Song, K.; Kim, J.; Lee, C.; Lee, J. PET Fabric/Polypyrrole Composite with High Electrical Conductivity for EMI Shielding. *Synth. Met.* **2002**, *126*, 233–239.
- (24) Zhang, X.; Huang, Y.; Liu, P. Enhanced Electromagnetic Wave Absorption Properties of Poly(3, 4-ethylenedioxythiophene) Nanofiber-Decorated Graphene Sheets by Non-covalent Interactions. *Nano-Micro Lett.* **2016**, *8*, 131–136.
- (25) Liu, X.; Sun, X.; Wang, Z.; Shen, X.; Wu, Y.; Kim, J.-K. Planar Porous Graphene Woven Fabric/Epoxy Composites with Exceptional Electrical, Mechanical Properties, and Fracture Toughness. *ACS Appl. Mater. Interfaces* **2015**, *7*, 21455–21464.
- (26) Jia, J.; Sun, X.; Lin, X.; Shen, X.; Mai, Y.-W.; Kim, J.-K. Exceptional Electrical Conductivity and Fracture Resistance of 3D Interconnected Graphene Foam/Epoxy Composites. *ACS Nano* **2014**, *8*, 5774–5783.
- (27) Ju, H.; Kim, M.; Kim, J. Thermoelectric Behavior of Poly(3, 4-ethylenedioxythiophene)/Graphene Composites Depending on Benzenesulfonate Derivatives Doped in Polymer Chains. *J. Mater. Sci.: Mater. Electron.* **2015**, *26*, 2544–2554.
- (28) Geng, Y.; Liu, M. Y.; Li, J.; Shi, X. M.; Kim, J. K. Effects of Surfactant Treatment on Mechanical and Electrical Properties of CNT/Epoxy Nanocomposites. *Composites, Part A* **2008**, *39*, 1876–1883.
- (29) Zhang, L.; Alvarez, N. T.; Zhang, M.; Haase, M.; Malik, R.; Mast, D.; Shanov, V. Preparation and Characterization of Graphene Paper for Electromagnetic Interference Shielding. *Carbon* **2015**, *82*, 353–359.
- (30) Lin, X.; Shen, X.; Zheng, Q.; Yousefi, N.; Ye, L.; Mai, Y.-W.; Kim, J.-K. Fabrication of Highly-Aligned, Conductive, and Strong Graphene Papers Using Ultralarge Graphene Oxide Sheets. *ACS Nano* **2012**, *6*, 10708–10719.
- (31) Ma, P.-C.; Zheng, Q.-B.; Mäder, E.; Kim, J.-K. Behavior of Load Transfer in Functionalized Carbon Nanotube/Epoxy Nanocomposites. *Polymer* **2012**, *53*, 6081–6088.

- (32) Ma, P.-C.; Mo, S.-Y.; Tang, B.-Z.; Kim, J.-K. Dispersion, Interfacial Interaction and Re-agglomeration of Functionalized Carbon Nanotubes in Epoxy Composites. *Carbon* **2010**, *48*, 1824–1834.
- (33) Shen, B.; Zhai, W.; Chen, C.; Lu, D.; Wang, J.; Zheng, W. Melt Blending In situ Enhances the Interaction Between Polystyrene and Graphene through π - π Stacking. *ACS Appl. Mater. Interfaces* **2011**, *3*, 3103–3109.
- (34) Hunter, C. A.; Sanders, J. K. The Nature of π - π Interactions. *J. Am. Chem. Soc.* **1990**, *112*, 5525–5534.
- (35) Pimenta, M.; Dresselhaus, G.; Dresselhaus, M. S.; Cancado, L.; Jorio, A.; Saito, R. Studying Disorder in Graphite-Based Systems by Raman Spectroscopy. *Phys. Chem. Chem. Phys.* **2007**, *9*, 1276–1290.
- (36) Reyes-Reyes, M.; Cruz-Cruz, I.; López-Sandoval, R. Enhancement of the Electrical Conductivity in PEDOT: PSS Films by the Addition of Dimethyl Sulfate. *J. Phys. Chem. C* **2010**, *114*, 20220–20224.
- (37) Wang, Z.; Shen, X.; Akbari Garakani, M.; Lin, X.; Wu, Y.; Liu, X.; Sun, X.; Kim, J. K. Graphene Aerogel/Epoxy Composites with Exceptional Anisotropic Structure and Properties. *ACS Appl. Mater. Interfaces* **2015**, *7*, 5538–5549.
- (38) Sriprachubwong, C.; Karuwan, C.; Wisitsorrot, A.; Phokharatkul, D.; Lomas, T.; Sritongkham, P.; Tuantranont, A. Inkjet-Printed Graphene-PEDOT:PSS Modified Screen Printed Carbon Electrode for Biochemical Sensing. *J. Mater. Chem.* **2012**, *22*, 5478–5485.
- (39) Wu, Y.; Lin, X.; Shen, X.; Sun, X.; Liu, X.; Wang, Z.; Kim, J.-K. Exceptional Dielectric Properties of Chlorine-Doped Graphene Oxide/Poly (vinylidene fluoride) Nanocomposites. *Carbon* **2015**, *89*, 102–112.
- (40) Yang, D.-Q.; Hennequin, B.; Sacher, E. XPS Demonstration of π - π Interaction Between Benzyl Mercaptan and Multiwalled Carbon Nanotubes and Their Use in the Adhesion of Pt Nanoparticles. *Chem. Mater.* **2006**, *18*, 5033–5038.
- (41) Wu, J.; Li, C.; Wang, D.; Gui, M. Damping and Sound Absorption Properties of Particle Reinforced Al Matrix Composite Foams. *Compos. Sci. Technol.* **2003**, *63*, 569–574.
- (42) Li, N.; Huang, Y.; Du, F.; He, X.; Lin, X.; Gao, H.; Ma, Y.; Li, F.; Chen, Y.; Eklund, P. C. Electromagnetic Interference (EMI) Shielding of Single-Walled Carbon Nanotube Epoxy Composites. *Nano Lett.* **2006**, *6*, 1141–1145.
- (43) Song, W.-L.; Cao, M.-S.; Lu, M.-M.; Bi, S.; Wang, C.-Y.; Liu, J.; Yuan, J.; Fan, L.-Z. Flexible Graphene/Polymer Composite Films in Sandwich Structures for Effective Electromagnetic Interference Shielding. *Carbon* **2014**, *66*, 67–76.
- (44) Liu, C.-D.; Lee, S.-N.; Ho, C.-H.; Han, J.-L.; Hsieh, K.-H. Electrical Properties of Well-Dispersed Nanopolyaniline/Epoxy Hybrids Prepared Using An Absorption-Transferring Process. *J. Phys. Chem. C* **2008**, *112*, 15956–15960.
- (45) Zhang, X.; Wei, S.; Haldolaarachchige, N.; Colorado, H. A.; Luo, Z.; Young, D. P.; Guo, Z. Magneto-resistive Conductive Polyaniline–Barium Titanate Nanocomposites with Negative Permittivity. *J. Phys. Chem. C* **2012**, *116*, 15731–15740.
- (46) Wei, S.; Mavinakuli, P.; Wang, Q.; Chen, D.; Asapu, R.; Mao, Y.; Haldolaarachchige, N.; Young, D. P.; Guo, Z. Polypyrrole-Titanium Nanocomposites Derived from Different Oxidants. *J. Electrochem. Soc.* **2011**, *158*, 205–212.
- (47) Zhu, J.; Zhang, X.; Haldolaarachchige, N.; Wang, Q.; Luo, Z.; Ryu, J.; Young, D. P.; Wei, S.; Guo, Z. Polypyrrole Metacomposites with Different Carbon Nanostructures. *J. Mater. Chem.* **2012**, *22*, 4996–5005.
- (48) Joo, J.; Oh, E.; Min, G.; MacDiarmid, A.; Epstein, A. J. Evolution of the Conducting State of Polyaniline from Localized to Mesoscopic Metallic to Intrinsic Metallic Regimes. *Synth. Met.* **1995**, *69*, 251–254.
- (49) Zhou, X.; Zhao, X. Resonant Condition of Unitary Dendritic Structure with Overlapping Negative Permittivity and Permeability. *Appl. Phys. Lett.* **2007**, *91*, 181908.
- (50) Smith, D. R.; Kroll, N. Negative Refractive Index in Left-Handed Materials. *Phys. Rev. Lett.* **2000**, *85*, 2933.
- (51) Kozyrev, A.; Van Der Weide, D. Nonlinear Left-Handed Transmission Line Metamaterials. *J. Phys. D: Appl. Phys.* **2008**, *41*, 173001.
- (52) Singh, K.; Ohlan, A.; Pham, V. H.; Balasubramanian, R.; Varshney, S.; Jang, J.; Hur, S. H.; Choi, W. M.; Kumar, M.; Dhawan, S. Nanostructured Graphene/Fe₃O₄ Incorporated Polyaniline as A High Performance Shield Against Electromagnetic Pollution. *Nanoscale* **2013**, *5*, 2411–2420.
- (53) Singh, A. P.; Garg, P.; Alam, F.; Singh, K.; Mathur, R.; Tandon, R.; Chandra, A.; Dhawan, S. Phenolic Resin-Based Composite Sheets Filled with Mixtures of Reduced Graphene Oxide, γ -Fe₂O₃ and Carbon Fibers for Excellent Electromagnetic Interference Shielding in the X-Band. *Carbon* **2012**, *50*, 3868–3875.
- (54) Arjmand, M.; Apperley, T.; Okoniewski, M.; Sundararaj, U. Comparative Study of Electromagnetic Interference Shielding Properties of Injection Molded Versus Compression Molded Multi-Walled Carbon Nanotube/Polystyrene Composites. *Carbon* **2012**, *50*, 5126–5134.
- (55) Al-Saleh, M. H.; Saadeh, W. H.; Sundararaj, U. EMI Shielding Effectiveness of Carbon Based Nanostructured Polymeric Materials: A Comparative Study. *Carbon* **2013**, *60*, 146–156.
- (56) Hsiao, S.-T.; Ma, C.-C. M.; Tien, H.-W.; Liao, W.-H.; Wang, Y.-S.; Li, S.-M.; Huang, Y.-C. Using A Non-covalent Modification to Prepare A High Electromagnetic Interference Shielding Performance Graphene Nanosheet/Water-Borne Polyurethane Composite. *Carbon* **2013**, *60*, 57–66.
- (57) Crespo, M.; González, M.; Elías, A. L.; Pulickal Rajukumar, L.; Baselga, J.; Terrones, M.; Pozuelo, J. Ultra-Light Carbon Nanotube Sponge as An Efficient Electromagnetic Shielding Material in the GHz Range. *Phys. Status Solidi RRL* **2014**, *8*, 698–704.
- (58) Moglie, F.; Micheli, D.; Laurenzi, S.; Marchetti, M.; Primiani, V. M. Electromagnetic Shielding Performance of Carbon Foams. *Carbon* **2012**, *50*, 1972–1980.
- (59) Kumar, R.; Dhakate, S. R.; Gupta, T.; Saini, P.; Singh, B. P.; Mathur, R. B. Effective Improvement of the Properties of Light Weight Carbon Foam by Decoration with Multi-Wall Carbon Nanotubes. *J. Mater. Chem. A* **2013**, *1*, 5727–5735.
- (60) Yang, Y.; Gupta, M. C.; Dudley, K. L.; Lawrence, R. W. Novel Carbon Nanotube-Polystyrene Foam Composites for Electromagnetic Interference Shielding. *Nano Lett.* **2005**, *5*, 2131–2134.
- (61) Yan, D.-X.; Ren, P.-G.; Pang, H.; Fu, Q.; Yang, M.-B.; Li, Z.-M. Efficient Electromagnetic Interference Shielding of Lightweight Graphene/Polystyrene Composite. *J. Mater. Chem.* **2012**, *22*, 18772–18774.
- (62) Zhang, H.-B.; Yan, Q.; Zheng, W.-G.; He, Z.; Yu, Z.-Z. Tough Graphene–Polymer Microcellular Foams for Electromagnetic Interference Shielding. *ACS Appl. Mater. Interfaces* **2011**, *3*, 918–924.
- (63) Wang, H.; Zheng, K.; Zhang, X.; Ding, X.; Zhang, Z.; Bao, C.; Guo, L.; Chen, L.; Tian, X. 3D Network Porous Polymeric Composites with Outstanding Electromagnetic Interference Shielding. *Compos. Sci. Technol.* **2016**, *125*, 22–29.
- (64) Chaudhary, A.; Kumari, S.; Kumar, R.; Teotia, S.; Singh, B. P.; Singh, A. P.; Dhawan, S.; Dhakate, S. R. Lightweight and Easily Foldable MCMB-MWCNTs Composite Paper with Exceptional Electromagnetic Interference Shielding. *ACS Appl. Mater. Interfaces* **2016**, *8*, 10600–10608.
- (65) Farhan, S.; Wang, R.; Li, K. Electromagnetic Interference Shielding Effectiveness of Carbon Foam Containing In situ Grown Silicon Carbide Nanowires. *Ceram. Int.* **2016**, *42*, 11330–11340.
- (66) Li, Y.; Shen, B.; Pei, X.; Zhang, Y.; Yi, D.; Zhai, W.; Zhang, L.; Wei, X.; Zheng, W. Ultrathin Carbon Foams for Effective Electromagnetic Interference Shielding. *Carbon* **2016**, *100*, 375–385.

NOTE ADDED AFTER ASAP PUBLICATION

This paper was published on March 2, 2017, with errors in equations 4 and 5. The corrected version was reposted on March 6, 2017.